Single-Ended Differential Protection in MTDC Networks using Optical Sensors

D. Tzelepis, *Student Member, IEEE,* A. Dyśko, *Member, IEEE,* G. Fusiek, *Member, IEEE,*
J. Nelson, P. Niewczas, *Member, IEEE,* D. Vozikis, *Student Member, IEEE,* P. Orr, N. Gordon, and C. Booth

***Abstract*—This paper presents a method for rapid detection of faults on VSC multi-terminal HVDC transmission networks using multi-point optical current sensing. The proposed method uses differential protection as a guiding principle, and is implemented using current measurements obtained from optical current sensors distributed along the transmission line. Performance is assessed through detailed transient simulation using Matlab/Simulink® models, integrating inductive DC-line terminations, detailed DC circuit breaker models and a network of fiber-optic current sensors. Moreover, the feasibility and required performance of optical-based measurements is validated through laboratory testing. Simulation results demonstrate that the proposed protection algorithm can effectively, and within very short period of time, discriminate between faults on the protected line (internal faults), and those occurring on adjacent lines or busbars (external faults). Hardware tests prove that the scheme can be achieved with the existing, available sensing technology.**

***Index Terms*—HVDC Protection, Multi-Terminal Direct Current, Modular Multi-level Converters, Optical Sensors.**

I. Introduction

DC side faults in high voltage direct current (HVDC) systems are characterized by large inrush currents with extremely high rates of rise caused by the discharge of trapped energy in the system capacitances. These include lumped DC capacitors installed on the DC side of the voltage source converters (VSCs), transmission line capacitances [1], and also the sub-module capacitors contained within modular multi-level converters (MMCs) [2], [3]. When faults occur in multi-terminal HVDC grids the DC protection system is expected to minimize the effects of the fault by disconnecting only the faulted section while permitting the remaining healthy part of the grid to continue normal operation [2]. Such requirements introduce the need for transient DC fault characterization [3], [4] and subsequent development of a discriminative, fast, sensitive and reliable DC protection method [5].

This paper deals with the challenges involved in protecting multi terminal direct current (MTDC) grids. The application of a distributed optical sensing system is proposed to achieve fast fault detection, enhanced reliability and discrimination. The key novel contribution of the paper is a new method termed *single-end differential protection* which is described in detail and validated using both transient simulation as well as laboratory testing. The paper is organized as follows: Section II presents the key aspects of HVDC protection, analyzing the challenges, existing detection methods and isolating devices. Section III proposes a new scheme for fast DC fault detection and faulted line discrimination. Section IV explains in detail the modelling approach. Section V introduces the Fiber Bragg Grating (FBG) based optical sensing technology for DC current measurement with emphasis given to distributed current sensing. In Section VI a number of performance assessment case studies are presented. Finally, in Section VII conclusions are drawn.

II. Protection in HVDC Systems

A. Detection Methods

For non-unit protection schemes there is a notable tendency towards the use of inductive termination on DC transmission lines. The deliberate inclusion of additional inductance not only limits the rate of change of DC current but also the resulting DC voltage signatures (and the fact that they may be different depending on fault location and known values of inserted inductance at line terminals) can help to achieve a discriminative non-unit type protection [2], [6], [7]. In [7] the derivative of DC voltage (measured on the line side of the inductor) is utilized to quickly detect and locate DC faults. However, the converter DC voltage immediately after the fault is assumed to remain unaffected, and highly resistive faults are not considered. In [6], a two-stage approach is proposed using an under-voltage element for fault detection, and a rate of change of voltage to enable selective tripping. Both methods in [6], [7] (which are notably non-unit) do not consider the influence of power reversal and the transmission medium (i.e. differences between overhead lines and cables). Such studies have been implemented in [2] where a different approach is adopted through using the rate of change of voltage measured at the DC reactor. A handshaking method is proposed in [8] to detect the faulted DC line. However the method can be considered slow and the fault isolation is achieved by AC breakers (again which will take several cycles to operate) which leads to de-energization of the converters. A detection method based on capacitor discharge is introduced in [9] to estimate the distance to fault. However, the performance of this method is poor under highly resistive faults. In [10] DC voltage signatures and over-currents are used to achieve an estimation of the fault-distance relationship. All of the methods presented in [8]–[10] only estimate the location of the faulted network branch, but the process of fault detection is not considered. A method based on travelling waves is proposed in [11]. This method utilizes derivatives of both voltage and current signals to determine whether the fault is internal or external. However, such method could be very sensitive to noise and lead to false indication of the fault. There are also a number of differential type schemes proposed in technical literature. For example, in [12], current measurements at both ends of each line are taken and the Discrete Wavelet Transform (DWT) is used in the protection algorithm. The discrimination between external and internal faults is achieved by comparing the energy of

the specific DWT components extracted from the current signals from both ends. In [13], another differential protection scheme is proposed using a comparison of the current of each line terminal and mechanical DC breakers. However, such methods assume the use of fault-tolerant converters in order to permit low-speed fault isolation. Additionally, it seems that the protection algorithm utilizes only one criterion which is a fixed predefined threshold. No other stages or criteria (e.g time delay or biasing) are included, which could make the algorithm vulnerable to noise and measurement uncertainties [14].

Some of the main challenges and drawbacks associated with differential protection include the inherent communication time delays, delays associated with encoding and decoding messages and correcting for latency of communications paths, and the reliability of the method if one of the measurements fails or the communications link is compromised. These challenges are overcome by the protection method proposed in this paper. This is explained and verified in Sections III and VI respectively.

B. Current Interruption Devices

The feasibility of operating secure MTDC networks relies largely on the ability to quickly interrupt DC-side fault currents, so that the operation of the healthy parts of the network is not compromised when one element of the network is faulted. The absence of a natural current zero crossing (as is the case with AC systems) requires a dedicated mechanism to drive the current to zero while dissipating the energy stored in the short circuit before the switching element can successfully interrupt the flow of current. There are many HVDC circuit breaker (CB) concepts proposed in the literature, however all have a similar structure, consisting of a commutation branch to drive the current to zero, a switching component for voltage withstand, and an absorption path for dissipating energy. Several breaker designs are proposed: solid state [15], hybrid [16], resonant [17] and superconducting [18].

III. Proposed Protection Method

The distributed optical sensing technology described in Section V formed the basis for the proposed *single-ended differential protection*.

A. Protection Strategy

The proposed protection strategy is explained using Fig. 1 where internal and external faults are illustrated. An internal fault is considered to be a fault within the protected element (i.e. DC Line 1 in this case) and an external fault is any fault outside the protected element. A series of current measuring sensors $S_1, S_2, ..., S_n$ are distributed along the line. These measurements can be accessed directly at either end of the line (the sensing locations are completely passive and require no power supply), where the optical interrogation, protective equipment and CBs are located. Due to close vicinity of these elements, it is assumed that the time delay between the decision making device (i.e. protection) and the CB can be ignored for the purposes of this study [13].

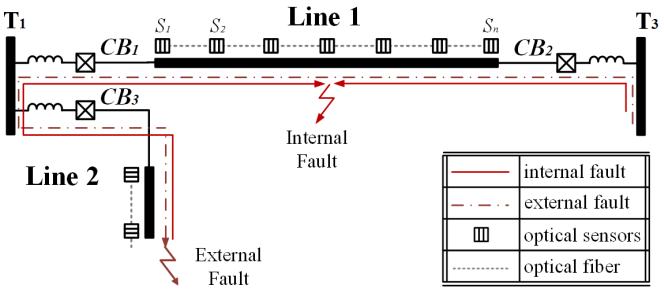

Fig. 1. Part of an MTDC network illustrating differential protection principle for external and internal faults.

A series of the differential currents are calculated using the measurements of two consecutive sensors according to equation (1).

$$\Delta i_{(k)}(t) = i_{s(k)}(t) - i_{s(k+1)}(t) \tag{1}$$

where $\Delta i_{(k)}(t)$ is the k-th differential current derived using the currents $i_{s(k)}$ and $i_{s(k+1)}$ measured at two adjacent sensors k and $k+1$ respectively ($k = 1, 2, ..., n-1$). During external faults the differential current $\Delta i_{(k)}(t)$ will be very close to zero while for internal faults a high differential value is expected. In order to ensure high sub-millisecond accuracy of the instantaneous differential current, the propagation time delay compensation is applied before the differential current is calculated as shown in equation (2). The amount of the compensation Δt is constant and is directly proportional to the distance between adjacent sensors S_k and S_{k+1} and speed of electromagnetic field propagation.

$$\Delta i_{(k)}(t) = i_{s(k)}(t - \Delta t) - i_{s(k+1)}(t) \tag{2}$$

The proposed algorithm is illustrated using a flowchart in Fig. 2. The protection logic has three stages. The first stage (depicted as Stage I) includes a differential current threshold comparison with a predefined value I_{TH}. To minimize the chances of protection instability caused by measurement errors, induced noise and/or transients during external faults, the value of the threshold needs to be carefully considered. Therefore, systematic iterative simulations have been performed with pole-to-pole (P-P) and pole-to-ground (P-G) faults at multiple locations on the transmission network model (including busbar faults), in order to establish the optimum current thresholds to be applied in Stage I and Stage II. Additionally, artificial noise was superimposed on the current measurements to verify the threshold selection and reduce the chance of spurious tripping.

The second stage (Stage II) is based on the rate of change of current. When the threshold I_{TH} is reached (Stage I) for a differential current $\Delta i_{(k)}$ the protection algorithm will look at the historical data of $di_{s(k)}/dt$ and $di_{s(k+1)}/dt$ using a short time window Δt_w. If any of the historical values of the derivatives $di_{s(k)}/dt(t-\Delta t_w)$ or $di_{s(k+1)}/dt(t-\Delta t_w)$ exceed a predefined threshold di/dt_{TH} the criterion for Stage II is fulfilled. Such stage ensures that the relay operating decision is reached purely as a result of a fault and not due to any short

signal disturbance (e.g. short spike should not be visible in the historical data). It was assumed that the window Δt_w=0.2 ms was adequate for this purpose. The third stage (Stage III) is included in the protection algorithm to ensure that protection operation does not result from any sensor failure. If no sensor failure is detected, Stage III initiates a tripping signal to the CB. This stage is explained better in Subsection VI-C.

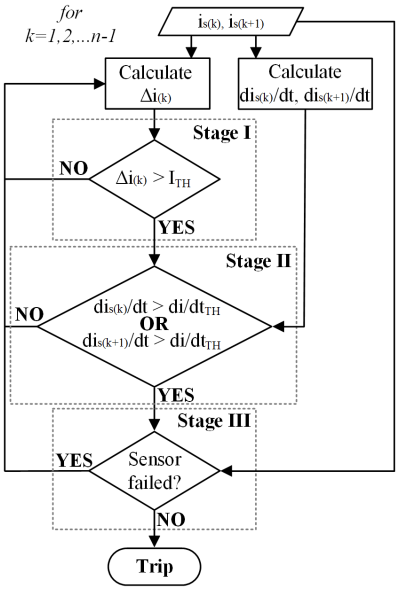

Fig. 2. Single-ended differential protection process.

B. Key Advantages

The proposed differential protection offers a number of significant advantages compared to conventional differential protection schemes, which typically require the use of time-consuming encoding and decoding at each line terminal in conjunction with dedicated communications schemes. These advantages are inherently achieved through the single-ended, multi-point sensing design of the proposed scheme.

Enhanced reliability: Considering a case of a sensor failure, the proposed method can still operate with a reduced number of sensors. This is not the case with a conventional differential protection which would be completely disabled should one of the measuring sensors fail. In this case, a back-up protection would take action which would reduce the speed of operation and potentially subject the system to higher and more sustained fault currents [13], [19].

Superior stability: During external faults the energy in cable capacitance discharges producing a short burst of differential current. With conventional DC differential protection (one measurement point for each cable termination) such a discharge can compromise protection stability especially with long transmission lines [20]. The differential current threshold would have to be increased, or additional delay introduced (as a "wait and see" strategy) which would reduce protection sensitivity and/or speed. Alternatively, such current would have to be compensated which requires extra computation, voltage measurements while the compensation is not always successful [20]. The proposed protection effectively eliminates the impact of cable capacitance by limiting the length of each protected element to the distance between two adjacent sensors.

High speed of operation: When an internal fault occurs, in conventional differential protection there is latency because of the travelling wave but also due to the time required for communicating the measured current to the remote end of the line [5], [13]. This time comprises encoding, time-tagging, latency and decoding. This time can amount to several milliseconds which in HVDC systems is long enough to allow currents to increase enough to exceed the breaking capability of the existing DC breakers [5]. Additionally, such overcurrents can seriously harm the diodes within the IGBTs of the converter during the freewheeling state [3], [10]. The worst case scenario is a close-up fault (also illustrated in Fig. 14) where the rate of change of current is the highest and the signal delay the longest (as it includes additional travelling wave delay to the remote end). Again, with the single-ended distributed sensing system there is no additional communication time delay, and the delays resulting from travelling waves are limited to the distance between two adjacent sensors, thus enabling ultra-high speed of protection operation.

The aforementioned key advantages of the proposed protection scheme are demonstrated with the aid of simulations in Section VI.

IV. Modelling

A. MTDC Network

A five-terminal HVDC grid has been utilized in all case studies as illustrated in Fig. 3. The system has been adopted from the Twenties Project case study on DC grids [21]. There are five MMCs operating at $\pm$400 kV (symmetric monopole), hybrid CBs and current limiting inductors at each transmission line end. The parameters of the AC and DC network components are described in detail in Table I.

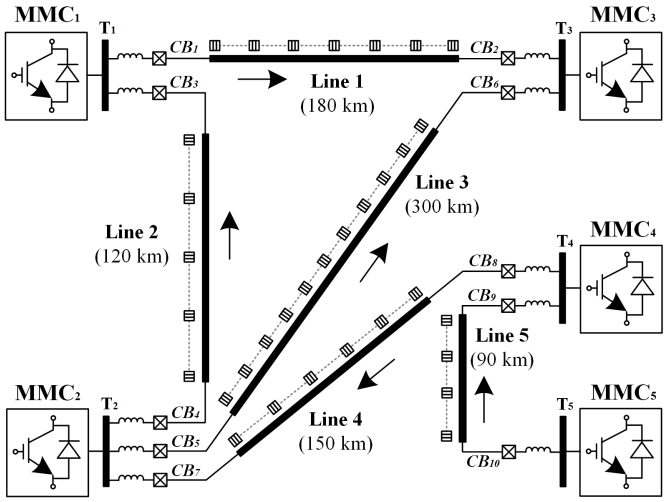

Fig. 3. Case study 5 terminal DC network integrating distributed sensing networks

On each transmission line, optical sensors are installed to accurately measure DC current every 30 km including

the terminals. Therefore, the numbers of DC current sensors are: seven, five, eleven, six and four on lines one to five respectively. The arrows indicate the direction of power flow from sending to receiving end of each line. It is emphasized that the proposed method is not direction-dependent. Sending/receiving end are used as a reference to better demonstrate the protection performance in the following sections.

TABLE I
DC AND AC NETWORK PARAMETERS

Parameter	Value
AC voltage $[V_{AC,L-L}]$	400 kV
AC frequency $[f_n]$	50 Hz
X/R ratio of AC networks	10
AC short-circuit level $[S_{s.c}]$	40 GVA
AC transformer reactance $[L_{TR}]$	0.2 p.u.
DC line external inductance $[L_{DC}]$	150 mH

B. Modular Multilevel Converters

The models of power converters utilized in this paper are based on 401-level Type 3 half bridge (HB) MMCs which have been developed according to guidelines and approaches described in [22]. Such representation has been validated against fully detailed models and has been demonstrated to accurately represent the converter behavior during steady-state, transient and fault conditions while remaining numerically stable and computationally efficient. Fig. 4 illustrates the Type 3 equivalent for one phase. The converter response is achieved through controlled voltage and current sources. A fault controller is also included which bypasses the submodules when the maximum current of the IGBTs is exceeded. In this case the converter behaves like an uncontrolled rectifier. Due to imbalanced voltage conditions, circulating currents are generated inside each MMC which increase current stress, introduce current distortion (arm currents), and produce additional conduction losses. To eliminate such currents a proportional resonant, circulating current suppression controller (PR-CCSC), as described in [23], has been integrated into the control system.

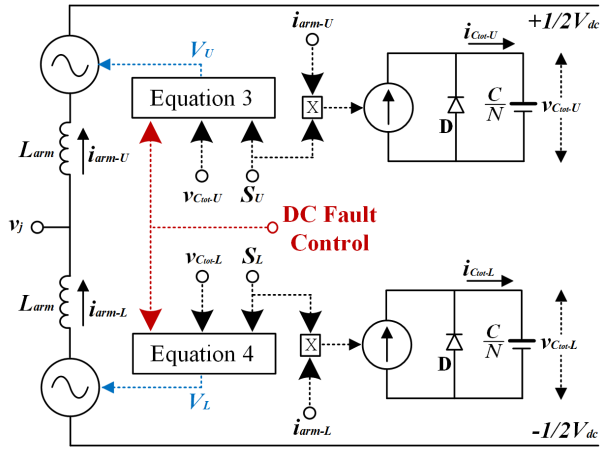

Fig. 4. Equivalent of the MMC Type 3 Model

The signals controlling voltage sources of the upper and lower arm (in each phase) can be expressed by equations (3) and (4) respectively.

$$V_U = S_U \; v_{Ctot-U} \tag{3}$$

$$V_L = S_L \; v_{Ctot-L} \tag{4}$$

S_U, S_L are the switching functions, while v_{Ctot-U} and v_{Ctot-L} are the total sums of capacitor voltages (for upper and lower arm respectively). Each MMC is operating at 800 kV ($\pm$400 kV), with an arm inductance of 0.1 p.u. and an equivalent arm capacitance of 20.84 μF.

C. Circuit Breaker

The HVDC CB model represents a hybrid design by ABB [24] as shown in Fig. 5. According to the manufacturer a breaking time of 2 ms is achievable while the maximum rating of the breaking current is 9 kA. During healthy operation the current flows through the fast mechanical disconnector and the load commutation switch. When a tripping signal is initiated, the load commutation switch opens driving the current through the commutation branch. This allows the fast mechanical disconnector to open, as no current is flowing through its contacts. In the next stage the commutation branch turns off, resulting in over-voltage which causes the surge arrester to operate. From this point the current flows through the surge arrester, where energy is dissipated and the current gradually falls to zero. For the purposes of DC CB modelling all power electronic devices have been modelled as ideal switches with zero resistance during their on-state. Additionally, a time delay of 2 ms has been added to represent the operation time of the breaker.

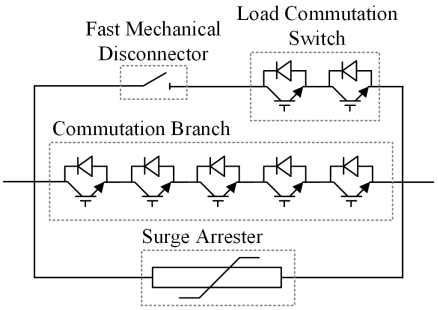

Fig. 5. Equivalent of Hybrid HVDC Breaker

D. Current Limiting Inductors

DC transmission lines are terminated with external inductances L_{DC} which limit the rate of rise of DC fault current di_{DC}/dt, and thus, provide additional fault detection time required by the protection system (before the CB maximum breaking current is reached). The inductor size was established assuming the maximum current of 9 kA, and the sum of all time delays before the current breaking begins calculated using equation (5).

$$t_{op} = t_{CB} + t_{meas} + t_{process} \tag{5}$$

where t_{CB} is the operating time of the hybrid CB (2 ms), t_{meas} is the delay associated with the remote measurement wave propagation, and $t_{process}$ is the time allocated to signal processing and decision making by the protective device.

For the calculation of time delays related to the remote measurements, equation (6) has been used. The worst case (longest delay) is a solid close-up fault (practically at 0km) which results in 60 km, a distance the remote measurement has to cover before it arrives at the local end (i.e. 30 km for the current wave to travel to the remote sensor, and 30 km for the measurement to travel back along the fiber optic cable). A refractive index of 1.4682 was assumed for SMF-28 fiber according to [25].

$$t_{meas} = \frac{2\ d_{2s}}{c/n} = \frac{60\ [km]}{\frac{299{,}792.5\ [km/s]}{1.4682}} \simeq 0.3\ [ms] \qquad (6)$$

where d_{2s} is the distance between two sensors, c is the speed of light in vacuum and n is the refraction index of optical fiber. Taking into account 1 ms for signal processing and decision making, the total estimated time delay is 3.3 ms. With 9 kA as the maximum breaking current and 3.3 ms as the total operation time t_{op}, the current rise rate di_{DC}/dt should be less than 2.73 kA/ms. Based on the proposed $\pm$400 kV network and for a solid fault at any busbar, the theoretical value of the inductor is calculated according to equation 7.

$$L_{DC} \geq \frac{\Delta V}{di_{DC}/dt} \geq \frac{400\ kV}{2.73\ kA/ms} \rightarrow L_{DC} \geq 146.5\ mH \quad (7)$$

where the L_{DC} is the inductor value, ΔV is the inductor voltage and di_{DC}/dt the DC current rise rate. For clarity, Fig. 6 illustrates simulation results for a P-P fault at busbar 1, trigerred at $t = 0$ ms with 2 ms post fault data for different inductance values.

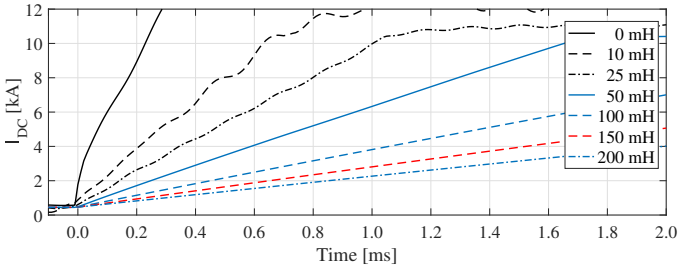

Fig. 6. Rate of rise of DC current with different inductance values, for P-P fault at busbar 1.

Table II presents the time required to reach 9 kA for the inductances illustrated in Fig. 6. As calculated by equation 7 it is therefore verified that the inductance value of 150 mH is the most appropriate option.

TABLE II
TIME INDICES AT 9 KA

Inductance [mH]	0	10	25	50	100	150	200
Time [ms]	0.22	0.60	0.93	1.49	2.70	3.97	5.31

V. OPTICAL SENSING TECHNOLOGY

Hybrid optical voltage and current sensors have previously been developed by the authors [26]–[28] to enable remote AC and DC voltage and current measurements in various metering and protection applications including distance and differential protection [29]–[32]. It will be shown in the following sections that the optical sensors technology is suitable for rapid detection of faults in HVDC circuits.

A. Fiber Bragg Gratings

Fiber Bragg Grating (FBG) sensors are formed by periodic modulation of the refractive index along an optical fiber core over a length of 5-20 mm. When such a structure is illuminated by a broadband light, it reflects a relatively narrow part of the incident light spectrum with a distinctive peak in the light intensity around the so called Bragg wavelength, λ_B. The spectral position of the peak is determined during the sensor fabrication process and described by the following relation:

$$\lambda_B = 2\ n_{eff}\ \Lambda \qquad (8)$$

where n_{eff} is the effective refractive index of the FBG section and Λ is the grating period. Any relative change in the grating period due to longitudinal elongation or contraction of the fiber causes spectral shift of the FBG peak. Since the refractive index of the fiber is a function of temperature, the FBG peak spectral position is also temperature dependent.

A relative change in the FBG peak wavelength, $\Delta\lambda_B/\lambda_B$, due to a change in strain, $\Delta\epsilon$, and temperature, ΔT, can be expressed by

$$\Delta\lambda_B = C_\epsilon \Delta\epsilon + C_T \Delta T \qquad (9)$$

where C_ϵ and C_T are the strain and temperature sensitivities [33].

B. Hybrid FBG-based voltage and current sensors

In this study, four FBGs inscribed in polyimide coated fibers, having a length of 7 mm, a bandwidth of 0.3 nm and peak wavelengths at 1539.60, 1551.56, 1554.72 and 1557.38 nm (as shown in Fig. 7) were utilized to build four hybrid low voltage sensors in order to prove the principle of the new protection scheme.

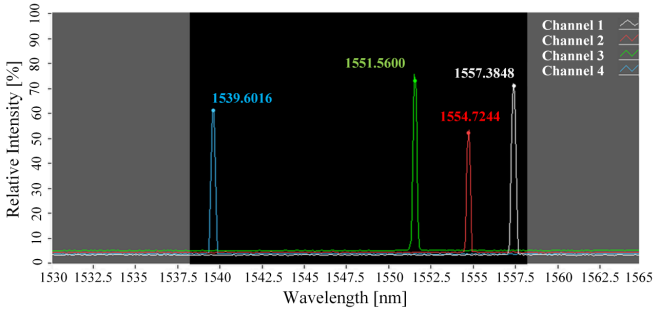

Fig. 7. FBGs spectra.

To construct a hybrid low voltage sensor, a 9 mm low voltage stack, P-883.11 PICMA from Physik Instrumente Ltd [34] having a maximum AC operating voltage of 30 V_{pk} (21.21 V_{rms}) was fixed between two alumina end blocks and an FBG sensor was pre-tensioned and epoxied to the ceramic blocks using EPO-TEK® 353ND. The sensor construction is shown in Fig. 8. Providing there is no mechanical stress in the

piezoelectric material, the strain (i.e. relative elongation $\Delta l/l$) induced by an external electric field is given by

$$\epsilon = d_{33}E = d_{33}\frac{V}{l} \tag{10}$$

where d_{33} is the longitudinal piezoelectric charge constant, E is the electric field, V is the voltage applied across the piezoelectric material and l is the length of the material [26].

A voltage applied across the stack generates strain which is exerted on the FBG producing a corresponding shift in its peak wavelength. Thus, the peak wavelength shift can be calibrated in terms of voltage [26].

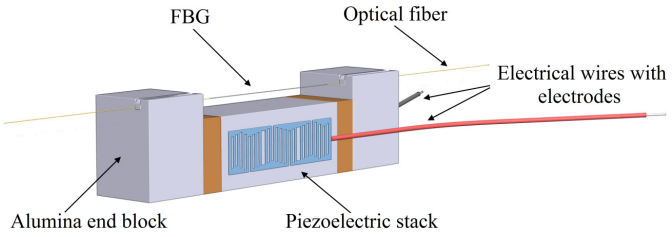

Fig. 8. Hybrid FBG-based voltage sensor.

By monitoring voltage across a burden resistor connected to the output of a conventional current transformer (CT), an AC optical current sensor can be realized whereby the FBG wavelength shift may be related to current [27]. Ultimately, by replacing a piezoelectric component with a magnetostrictive transducer, a DC current sensor can be realized [28], which would be a device of choice for the final deployment of this system. Light, composite insulators can be used to provide the means of guiding optical fiber between the sensors (installed directly on the conductor) and the pole which is at ground potential. Optical fiber would be provided in a trench alongside the HVDC transmission line, or in some cases may be integrated within the conductors or wrapped around conductors (very common in AC systems).

C. Experimental Setup

A diagram of the experimental set-up utilized for practical validation of the proposed scheme is shown in Fig. 9. For representative purposes and to manage expense associated with the experimental setup, four sensors have been used with the assumption that they are distributed evenly along the 300 km transmission line (DC Line 3 in the network shown in Fig. 3). Pre-simulated fault currents at corresponding four locations along the transmission line were used to produce replica voltage waveforms (generated directly from a multi-function data acquisition card). These voltage traces (which represent the DC line currents) were physically input to the optical sensors and the sampled data obtained from the optical interrogation system was stored on a PC for processing by the protection system algorithm developed in Simulink.

To simplify the experimental circuitry FBG optical voltage sensors were used instead of current sensors. The FBGs were optically connected to a commercial SmartScan interrogator (Smart Fibres) offering a scanning speed of 2.5 kHz over a spectral range of 1528-1568 nm. To increase the scanning

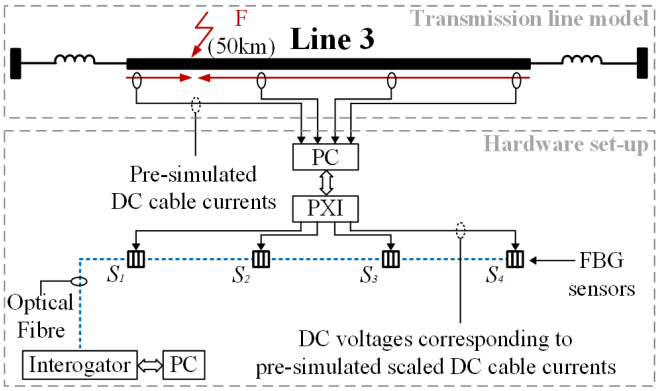

Fig. 9. Experimental setup diagram. Fault occurrence is shown between sensors S_1 and S_2 at 50 km.

speed, the device's maximum wavelength range was narrowed to 1538-1558 nm and the optical signals reflected from the sensors were acquired at a frequency of 5 kHz. A PXIe-8106 controller and a 16-bit PXIe-6259 data acquisition card (both from National Instruments) were used for generating signals utilized for driving the voltage sensors. The card offers 16 analogue inputs that can be scanned at a maximum sampling rate of 1.25 MS/s and 4 analogue outputs with a maximum update rate of 2.8 MS/s. The maximum DC voltage range for the input and output channels is ± 10 V.

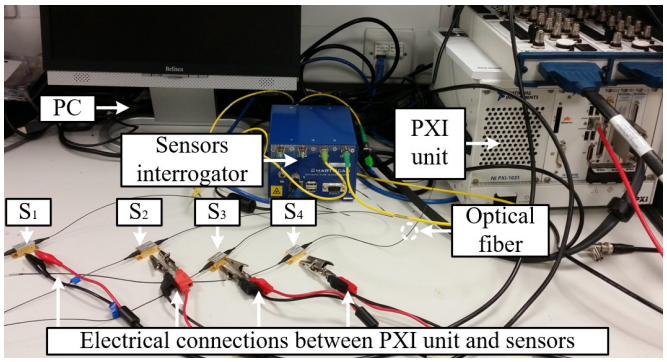

Fig. 10. Laboratory experimental setup.

To protect the piezoelectric component from depolarization and degradation due to overvoltage conditions, a transient voltage suppression (TVS) diode was connected between the component terminals (not shown in Fig. 8) [33].

Prior to testing the low voltage sensors were characterized and calibrated. A DC voltage was applied across the piezoelectric transducers in 1 V steps within a range of ± 10 V. The FBG peak wavelengths were then recorded for all corresponding voltages. The inverted function was then used to calibrate wavelength shifts in terms of voltage. The actual experimental setup is depicted in Fig. 10.

VI. Simulation and Experimental Results

In this section simulation results are presented which quantify the performance of the proposed protection scheme. All presented waveforms use the convention for current direction as indicated in Fig. 3.

A. Sensitivity to Internal Fault

In Fig. 11 the protection response to a fault occurring at 50 km from terminal T_1 on DC line 1 (internal fault) is illustrated. The fault is triggered at $t = 100$ ms. During this fault which is physically located between sensors S_2 and S_3, it can be seen that the differential current derived from the measurements of these two sensors is increasing rapidly (Fig. 11(a)), exceeding the protection threshold, and thus, fulfilling the first operation criterion. Since the fault is internal, it can be seen that prior to the fault detection the rate of change di_{DC}/dt for both currents (sensors S_2 and S_3) are non-zero (Fig. 11(b)) which indicates the satisfaction of the second criterion. A tripping signal is initiated by the third criterion (Stage III), however it is not illustrated here due to space limitations. The fault current interruption process is illustrated in Fig. 11(c) and Fig. 11(d) for sending and receiving end of DC Line 1 respectively. Before the breaker operates the current flows through the commutation branch. After the fast mechanical disconnector opens the current flows through the surge arrester where it gradually reduces to zero and the interruption process is finally complete. It can be seen that after the initiation of the tripping signal, it takes 2 ms for the breaker to operate.

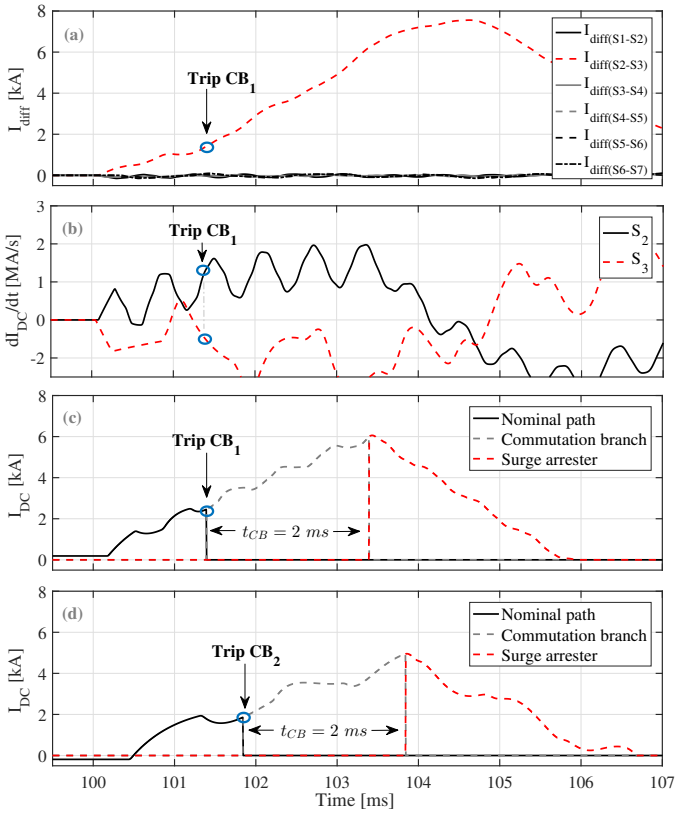

Fig. 11. P-P fault at DC Line 1. (a) Differential currents as seen by sending end of DC Line 1, (b) Rate of change of DC current for sensor S_2 and S_3 as seen by sending end of DC Line 1, (c) Fault current interruption in hybrid CB_1, (d) Fault current interruption in hybrid CB_2.

B. External fault

In order to demonstrate the superior stability mentioned in Subsection III-B an external busbar P-P fault (as seen by the protection system of DC Line 1) has been applied at T_3. Fig. 12 illustrates the differential currents as calculated by the proposed protection scheme (i.e. obtained from two adjacent sensors S_3 and S_4) and a conventional differential protection (i.e. two measuring points at opposite ends of the line).

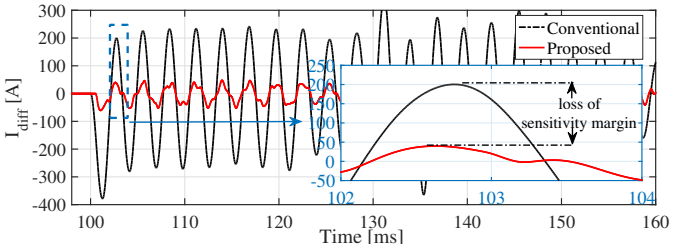

Fig. 12. Differential currents for external P-P busbar fault at T_3 as seen by the DC Line 1 protection.

During an external fault the cable capacitance between two measurement points discharges to the fault, producing a short temporary burst of differential current. The longer the distance between the measurement points, the higher the cable capacitance, hence the higher the magnitude of this temporary differential current. For the proposed protection scheme, such differential current is limited by the capacitance between two sensing points (i.e. 30 km) as demonstrated in Fig. 12. The differential current as calculated by a conventional differential protection scheme is much higher due to the inclusion of the entire line capacitance. In order for the protection system to remain stable during such external faults a threshold (and probably a time delay) is required to be included in the algorithm, which in the case of a conventional scheme would be much higher, leading to a sensitivity loss. DC busbar faults are assumed to be cleared by dedicated DC busbar protection and are not considered in this paper. Such faults are expected to be detected almost instantaneously, and the clearance time is only affected by the operation time of the DC breaker [13].

C. Sensor Failure

Fig. 13 depicts a case where the fourth sensor on DC Line 1 fails. This is emulated by artificially driving the current measurement to zero (worst case scenario) at $t = 100$ms. Such a change is expected to make an impact on all of the differential currents calculated measurements from the fourth sensor (i.e. $I_{diff(S3-S4)}$, $I_{diff(S4-S5)}$).

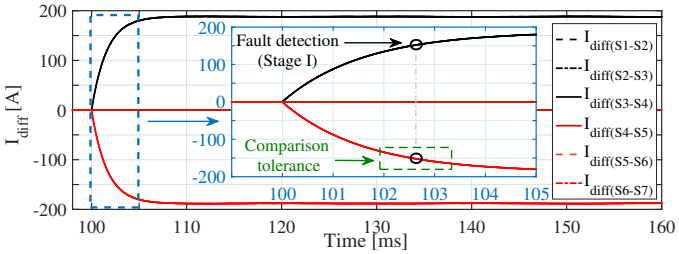

Fig. 13. Differential currents as seen by DC Line 1 protection considering a failure of the fourth sensor.

The key to detection of a sensor failure is the comparison of the differential current (e.g. $I_{diff(S3-S4)}$) at the time

instant when Stage I operates with an adjacent differential current ($I_{diff(S4-S5)}$). As Fig. 13 illustrates, such currents are expected to have similar amplitudes but opposite polarity. A comparison tolerance of $\pm 10\%$ is included to improve reliability of sensor failure detection. Consequently, no tripping has been observed in this case. This criterion is used in Stage III in the protection algorithm as illustrated in Fig. 2.

D. Speed of Operation

In order to demonstrate the advantage in operation speed a fault has been applied to DC Line 1 at a distance of 10 km from the sending end. The proposed protection scheme has been compared against a conventional differential scheme (as described in [13]) in terms of fault detection time and the maximum current flowing through the CB and the IGBTs of MMC_1. It is assumed that the conventional differential scheme utilizes two current measurements (one from each end of the line) and uses the same differential current threshold and transmission medium (with the same propagation speed) as is applied in the proposed scheme. Time delay associated with the conventional scheme was assumed to be 1.5 ms as illustrated in Fig. 14. Such delay corresponds to the time ($t_{prop.}$) required for the measured change in currents due to the fault propagating to the remote end R_2 and the time ($t_{com.}$) to send the measurement back to the local end R_1 via fiber optic cable. Additional delays associated with local signal processing have been ignored.

TABLE III
COMPARISON OF THE PROPOSED AND CONVENTIONAL DIFFERENTIAL PROTECTION SCHEME FOR A P-P FAULT AT 10 KM ON DC LINE 1

Protection scheme	CB trip time [ms]	Maximum current [kA]	
		CB	IGBT
Conventional	2.98	8.15	2.92
Proposed	1.32	7.08	2.13

The results in Table III clearly demonstrate the advantage of the proposed scheme both in terms of speed of operation and the current levels imposed upon the CB and IGBTs. Even though CBs and IGBTs can have their own dedicated protective system [10], [35] a reduced current and hence thermal stress is always favorable.

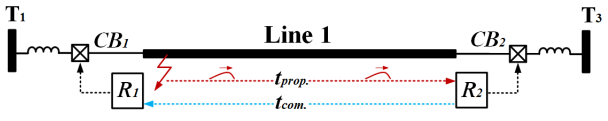

Fig. 14. Illustration of time delays associated with conventional differential scheme during close-up faults.

E. Fault Types

Tables IV and V illustrate simulation results for P-P and P-G faults respectively, for different distances along all transmission lines. It can be seen that in all cases only the required breakers operate, proving high selectivity of the scheme. It is also important to report that the CB current never exceeds 9 kA as required and discussed in section IV-C. This verifies the importance of the inductive terminations of the transmission lines. For P-G faults the protection system has been tested with ground fault resistances of up to 300 Ω and the protection scheme has been found to successfully and correctly operate in all cases.

TABLE IV
PROTECTION SYSTEM PERFORMANCE RESULTS FOR P-P FAULTS

Line	Distance [km]	Breakers operated	Sending end		Receiving end	
			CB trip time [ms]	CB max. current [kA]	CB trip time [ms]	CB max. current [kA]
1	1	CB_1, CB_2	1.329	7.45	2.075	4.07
	90	CB_1, CB_2	1.525	5.12	1.675	5.28
	120	CB_1, CB_2	1.677	5.41	1.525	5.82
	179	CB_1, CB_2	2.074	4.44	1.331	7.07
2	1	CB_3, CB_4	1.327	7.49	1.775	5.17
	25	CB_3, CB_4	1.280	6.47	1.730	5.00
	60	CB_3, CB_4	1.373	5.97	1.524	5.81
	119	CB_3, CB_4	1.774	5.56	1.326	7.06
3	1	CB_5, CB_6	1.328	7.44	2.076	4.10
	150	CB_5, CB_6	1.523	5.11	1.676	5.30
	250	CB_5, CB_6	1.674	5.38	1.526	5.83
	299	CB_5, CB_6	2.073	4.43	1.327	7.04
4	1	CB_7, CB_8	1.332	8.03	1.925	3.80
	75	CB_7, CB_8	1.521	6.46	1.520	4.75
	100	CB_7, CB_8	1.670	5.84	1.375	5.06
	149	CB_7, CB_8	1.928	5.46	1.323	6.44
5	1	CB_9, CB_{10}	1.325	7.33	1.630	5.20
	45	CB_9, CB_{10}	1.376	6.18	1.374	5.73
	89	CB_9, CB_{10}	1.631	5.64	1.330	6.98

TABLE V
PROTECTION SYSTEM PERFORMANCE RESULTS FOR P-G FAULTS

Line	Distance [km]	Breakers operated	Sending end		Receiving end	
			CB trip time [ms]	CB max. current [kA]	CB trip time [ms]	CB max. current [kA]
1	1	CB_1, CB_2	1.382	1.65	2.125	1.05
	90	CB_1, CB_2	1.565	1.40	1.715	1.12
	120	CB_1, CB_2	1.714	1.42	1.567	1.19
	179	CB_1, CB_2	2.128	1.38	1.380	1.43
2	1	CB_3, CB_4	1.377	2.12	1.820	0.98
	25	CB_3, CB_4	1.330	2.03	1.780	1.03
	60	CB_3, CB_4	1.420	1.84	1.566	1.04
	119	CB_3, CB_4	1.830	1.75	1.381	1.22
3	1	CB_5, CB_6	1.376	2.27	2.715	0.96
	150	CB_5, CB_6	1.865	1.67	2.015	1.09
	250	CB_5, CB_6	2.460	1.60	1.418	1.37
	299	CB_5, CB_6	2.725	1.50	1.388	1.47
4	1	CB_7, CB_8	1.385	2.35	1.975	0.82
	75	CB_7, CB_8	1.568	1.91	1.565	0.84
	100	CB_7, CB_8	1.717	2.02	1.416	0.94
	149	CB_7, CB_8	1.970	2.01	1.375	1.07
5	1	CB_9, CB_{10}	1.400	0.81	1.700	1.08
	45	CB_9, CB_{10}	1.415	0.74	1.414	1.13
	89	CB_9, CB_{10}	1.680	0.86	1.383	1.25

F. Transmission Line Length

In order to assess the potential effect of the line length on operation of the proposed scheme the length of DC Line 3 in the network shown in Fig. 3 has been modified to cover 600 km and 1200 km long power transmission. Table VI presents the results for P-P fault at different locations along the line. Similar results have been obtained for P-G faults, and therefore, these are not included in the paper due to space limitations.

In all cases only the CBs related to DC Line 3 operate (i.e CB_5 & CB_6) proving that the scheme preserves high level of selectivity and speed of operation, even with very long transmission lines.

TABLE VI
PROTECTION SYSTEM PERFORMANCE RESULTS FOR P-P FAULTS FOR LONGER DC CABLES

Length [km]	Distance [km]	Breakers operated	Sending end		Receiving end	
			CB trip time [ms]	CB max. current [kA]	CB trip time [ms]	CB max. current [kA]
600	5	CB_5, CB_6	1.330	6.48	4.165	2.18
	50	CB_5, CB_6	1.380	5.43	3.915	2.22
	150	CB_5, CB_6	1.830	4.08	3.470	2.36
	300	CB_5, CB_6	2.575	3.70	2.725	3.59
	400	CB_5, CB_6	3.170	3.07	2.125	3.96
	500	CB_5, CB_6	3.615	2.87	1.680	4.34
	595	CB_5, CB_6	4.165	2.43	1.330	6.16
1200	10	CB_5, CB_6	1.322	6.27	7.139	2.19
	50	CB_5, CB_6	1.380	5.39	6.900	2.24
	500	CB_5, CB_6	3.615	2.87	4.660	2.36
	600	CB_5, CB_6	4.065	2.53	4.215	2.41
	800	CB_5, CB_6	5.110	2.54	3.170	2.95
	1000	CB_5, CB_6	6.155	2.48	2.130	3.97
	1190	CB_5, CB_6	7.135	2.35	1.320	6.05

G. Experimental Results

The measured response of the optical sensors and the protection system to an internal fault at DC Line 3 occurring at 50 km is shown in Fig. 15. The recorded DC voltages are scaled down replicas of the DC Line currents which were pre-simulated and physically generated in real-time using a data acquisition card within its output range of $\pm 10\,\mathrm{V}$ (refer to Fig. 15(a)). These voltages were then recorded by the FBG-based voltage sensors as shown in Fig. 15(b). The differential voltages shown in Fig. 15(c) (corresponding to the differential currents in the primary power system) were calculated and used for fault detection according to the proposed algorithm.

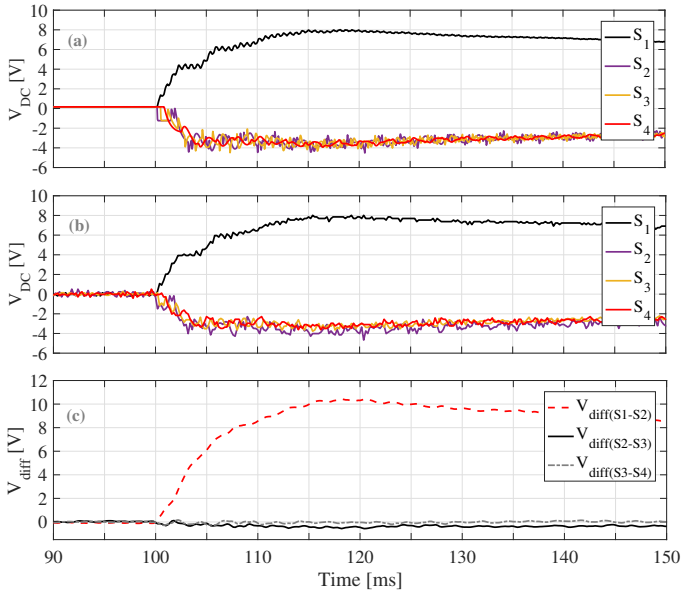

Fig. 15. FBG and protection response for pre-simulated fault at line 3 at 50km. (a) DC voltages corresponding to scaled DC cable currents, (b) FBG sensor voltages, (c) Differential voltages based on FBG sensors.

VII. CONCLUSIONS

In this paper a new single-end differential protection scheme has been described which utilizes the principle of distributed optical sensing. It has been found that the proposed scheme can correctly operate for all types of faults, providing fast and discriminative protection for HVDC transmission systems. This has been demonstrated in detailed transient simulation, and further validated using a scaled down laboratory prototype of the proposed differential scheme. The key advantages of single-ended instantaneous current measurement have been outlined which result in enhanced reliability, superior stability, and high speed of operation. The design, construction and operating principles of the hybrid optical sensors have been discussed in the paper with specific emphasis on the practical aspects of implementing such sensors in distributed monitoring of transmission lines. In order to demonstrate the practical feasibility of the scheme, the pre-simulated fault current waveforms have been converted to analogue voltages on a multi-function data acquisition card, and coupled directly to four optical voltage sensors during the experiments, imitating a scheme with four measuring points distributed along a 300 km DC transmission line. The response of the optical sensors and the protection system to an internal fault at DC line 3 (occurring 50 km from the sending end of the line) have proven that the proposed protection scheme is suitable for rapid fault detection and can, therefore, be considered as a viable option for protection of future HVDC circuits, including multi-terminal systems.

ACKNOWLEDGMNETS

Research presented in this paper was supported by GE Solutions Ltd, the Innovate UK (TSB Project Number 102594) and the European Metrology Research Programme (EMRP) - ENG61. The EMRP is jointly funded by the EMRP participating countries within EURAMET and the European Union.

REFERENCES

[1] M. K. Bucher and C. M. Franck, "Analytic approximation of fault current contributions from capacitive components in HVDC cable networks," *IEEE Trans. on Power Delivery*, vol. 30, no. 1, pp. 74–81, Feb 2015.
[2] R. Li, L. Xu, and L. Yao, "DC fault detection and location in meshed multi-terminal HVDC systems based on DC reactor voltage change rate," *IEEE Trans. on Power Delivery*, no. 99, 2016.
[3] D. Tzelepis, S. Ademi, D. Vozikis, A. Dysko, S. Subramanian, and H. Ha, "Impact of VSC converter topology on fault characteristics in HVDC transmission systems," in *Power Electronics Machines and Drives, IET 8th International Conference on*, March 2016.
[4] E. Kontos, R. Pinto, S. Rodrigues, and P. Bauer, "Impact of HVDC transmission system topology on multiterminal DC network faults," *IEEE Trans. on Power Delivery*, vol. 30, no. 2, pp. 844–852, April 2015.
[5] CIGRE, "HVDC grid feasibility study," Tech. Rep., April 2013.
[6] W. Leterme, J. Beerten, and D. Van Hertem, "Non-unit protection of HVDC grids with inductive DC cable termination," *IEEE Trans. on Power Delivery*, vol. PP, no. 99, pp. 1–1, 2015.
[7] J. Sneath and A. Rajapakse, "Fault detection and interruption in an earthed HVDC grid using rocov and hybrid DC breakers," *IEEE Trans. on Power Delivery*, vol. PP, no. 99, pp. 1–1, 2014.
[8] L. Tang and B.-T. Ooi, "Locating and isolating DC faults in multi-terminal DC systems," *Power Delivery, IEEE Trans. on*, vol. 22, no. 3, pp. 1877–1884, July 2007.
[9] J. Yang, J. Fletcher, and J. O'Reilly, "Short-circuit and ground fault analyses and location in VSC-based DC network cables," *Industrial Electronics, IEEE Trans. on*, vol. 59, no. 10, pp. 3827–3837, Oct 2012.
[10] ——, "Multiterminal DC wind farm collection grid internal fault analysis and protection design," *IEEE Trans. on Power Delivery*, vol. 25, no. 4, pp. 2308–2318, Oct 2010.
[11] J. Wang, B. Berggren, K. Linden, and J. Pan, "Multi-terminal DC system line protection requirement and high speed protection solutions," *CIGRE*, pp. 1–9, 2015.

[12] A. E. Abu-Elanien, A. A. Elserougi, A. S. Abdel-Khalik, A. M. Massoud, and S. Ahmed, "A differential protection technique for multi-terminal HVDC," *Electric Power Systems Research*, vol. 130, pp. 78 – 88, 2016.

[13] M. Hajian, L. Zhang, and D. Jovcic, "DC transmission grid with low-speed protection using mechanicalDC circuit breakers," *IEEE Trans. on Power Delivery*, vol. 30, no. 3, pp. 1383–1391, June 2015.

[14] S. Fletcher, P. Norman, K. Fong, S. Galloway, and G. Burt, "High-speed differential protection for smart DC distribution systems," *Smart Grid, IEEE Trans. on*, vol. 5, no. 5, pp. 2610–2617, Sept 2014.

[15] M. Hajian, D. Jovcic, and B. Wu, "Evaluation of semiconductor based methods for fault isolation on high voltage DC grids," *IEEE Trans. on Smart Grid*, vol. 4, no. 2, pp. 1171–1179, June 2013.

[16] C. Meyer, M. Kowal, and R. De Doncker, "Circuit breaker concepts for future high-power DC-applications," in *Industry Applications Conference, Fourtieth IAS Annual Meeting. Conference Record of the*, vol. 2, Oct 2005, pp. 860–866.

[17] M. Bucher and C. Franck, "Fault current interruption in multiterminal HVDC networks," *IEEE Trans. on Power Delivery*, vol. PP, no. 99, pp. 1–1, 2015.

[18] B. Xiang, Z. Liu, Y. Geng, and S. Yanabu, "DC circuit breaker using superconductor for current limiting," *IEEE Trans. on Applied Superconductivity*, vol. 25, no. 2, pp. 1–7, April 2015.

[19] W. Leterme, S. P. Azad, and D. V. Hertem, "A local backup protection algorithm for HVDC grids," *IEEE Trans. on Power Delivery*, vol. PP, no. 99, pp. 1–1, 2016.

[20] H. Takeda, H. Ayakawa, M. Tsumenaga, and M. Sanpei, "New protection method for hvdc lines including cables," *IEEE Trans. on Power Delivery*, vol. 10, no. 4, pp. 2035–2039, Oct 1995.

[21] EU, "Twenties project - final report," Tech. Rep., Oct 2013.

[22] H. Saad, S. Dennetire, J. Mahseredjian, P. Delarue, X. Guillaud, J. Peralta, and S. Nguefeu, "Modular multilevel converter models for electromagnetic transients," *IEEE Trans. on Power Delivery*, vol. 29, no. 3, pp. 1481–1489, June 2014.

[23] S. Li, X. Wang, Z. Yao, T. Li, and Z. Peng, "Circulating current suppressing strategy for MMC-HVDC based on nonideal proportional resonant controllers under unbalanced grid conditions," *IEEE Trans. on Power Electronics*, vol. 30, no. 1, pp. 387–397, Jan 2015.

[24] M. Callavik, A. Blomberg, J. Hafner, and B. Jacobson, "The hybrid HVDC breaker," in *ABB Grid Systems*, November 2012.

[25] J. D. Shin and J. Park, "Plastic optical fiber refractive index sensor employing an in-line submillimeter hole," *IEEE Photonics Technology Letters*, vol. 25, no. 19, pp. 1882–1884, Oct 2013.

[26] L. Dziuda, P. Niewczas, G. Fusiek, and J. R. McDonald, "Hybrid fiber optic voltage sensor for remote monitoring of electrical submersible pump motors," *Optical Engineering*, vol. 44, no. 6, pp. 064 401–064 401–6, 2005.

[27] L. Dziuda, G. Fusiek, P. Niewczas, G. Burt, and J. McDonald, "Laboratory evaluation of the hybrid fiber-optic current sensor," *Sensors and Actuators A: Physical*, vol. 136, no. 1, pp. 184–190, may 2007.

[28] D. Reilly, A. J. Willshire, G. Fusiek, P. Niewczas, J. R. Mcdonald, and M. Ieee, "A Fiber-Bragg-Grating-Based Sensor for Simultaneous AC Current and Temperature Measurement," *IEEE Sensors Journal*, vol. 6, no. 6, pp. 1539–1542, 2006.

[29] P. Orr, G. Fusiek, P. Niewczas, A. Dyko, C. Booth, F. Kawano, and G. Baber, "Distributed optical distance protection using fbg-based voltage and current transducers," *2011 IEEE Power and Energy Society General Meeting*, pp. 1–5, July 2011.

[30] P. Orr, G. Fusiek, C. D. Booth, P. Niewczas, A. Dyko, F. Kawano, P. Beaumont, and T. Nishida, "Flexible protection architectures using distributed optical sensors," in *Developments in Power Systems Protection, 11th International Conference on*, April 2012, pp. 1–6.

[31] P. Orr, C. Booth, G. Fusiek, P. Niewczas, A. Dysko, F. Kawano, and P. Beaumont, "Distributed photonic instrumentation for smart grids," in *Applied Measurements for Power Systems,IEEE International Workshop on*, Sept 2013, pp. 63–67.

[32] P. Orr, G. Fusiek, P. Niewczas, C. D. Booth, A. Dyko, F. Kawano, T. Nishida, and P. Beaumont, "Distributed photonic instrumentation for power system protection and control," *IEEE Transactions on Instrumentation and Measurement*, vol. 64, no. 1, pp. 19–26, Jan 2015.

[33] G. Fusiek, J. Nelson, P. Orr, P. Niewczas, and C. Booth, "Frequency characterisation of an optically-interrogated rogowski coil for smart grid protection applications," *SENSORS, 2015 IEEE*, pp. 1–4, Nov 2015.

[34] Corning-Inc., "SMF-28® ultra optical fiber," www.corning.com/media/worldwide/coc/documents/Fiber/SMF-28%20Ultra.pdf, [25-10-2016].

[35] W. Lin, D. Jovcic, S. Nguefeu, and H. Saad, "Modelling of high-power hybrid dc circuit breaker for grid-level studies," *IET Power Electronics*, vol. 9, no. 2, pp. 237–246, 2016.

Dimitrios Tzelepis (S'13) received the B.Eng. in Electrical Engineering and the M.Sc in Wind Energy Systems from Technological Education Institution of Athens (2013) and University of Strathclyde (2014) respectively. He is currently pursuing his Ph.D. at the department of Electronic and Electrical Engineering, University of Strathclyde, Glasgow, U.K. His main research interests include power systems protection, relay algorithms, application of advanced signal analysis in protection and fault location applications and HVDC protection and fault location.

Adam Dyśko (M'06) is currently a Senior Lecturer in the Department of Electronic and Electrical Engineering, University of Strathclyde. His main research areas are power power system protection, system control and stability, and power quality

Grzegorz Fusiek received the M.Sc. degree in Electrical Engineering from the Lublin University of Technology, Poland, in 2000 and the Ph.D. degree in the area of interrogation systems for spectrally encoded sensors from the University of Strathclyde, Glasgow, UK, in 2007. He is a Research Fellow within the Institute for Energy and Environment in the Electronic and Electrical Engineering Department, University of Strathclyde. His interests concentrate on the optical sensing techniques for power industry and energy systems applications. He has published over 50 technical papers in this area.

John Nelson received the B.Sc. (Hons) and Ph.D. degrees in Physics from the University of Glasgow in 2000 and 2008 respectively. He has worked in the field of optical sensing at the University of Glasgow, Université Paris 7 and the University of Strathclyde. He currently works with the Advanced Sensors Team at the University of Strathclyde. His current research activities are focussed on developing novel optically-interrogated sensors for power systems protection.

Pawel Niewczas (M'05) is a Reader in the Department of Electronic and Electrical Engineering at the University of Strathclyde. He is leading the Advanced Sensors Team within the Institute for Energy and Environment in the same department. His main research interests centre on the advancement of photonic sensing methods and systems integration in applications that lie predominantly in power and energy sectors.

Dimitrios Vozikis (S'16) received the M.Sc from University of Strathclyde in 2014. He is currently working towards his Ph.D at the PEDEC group at University of Strathclyde. His main research interests include HVDC converters and power conversion.

Philip Orr received the B.En.g and Ph.D. degrees in electronic and electrical engineering in 2007 and 2011 respectively from the University of Strathclyde. He is currently Managing Director of Synaptec Ltd and an Honorary Researcher at the University of Strathclyde. His research focus is on the fundamental design and development of fiber-optic sensors and interrogators for power and energy system instrumentation.

Neil Gordon was awarded an M.Sci. in Physics at the University of Glasgow (2011) and a Ph.D. at the Institute for Gravitational Research (2015) in the field of advanced optical interferometric techniques for future gravitational wave detectors. As senior engineer at Synaptec Ltd his current research focus is on the development of fiber sensors and interrogators for application within power and energy systems.

Campbell Booth received the B.Eng. and Ph.D. degrees in electrical and electronic engineering from the University of Strathclyde, Glasgow, U.K., in 1991 and 1996, respectively. He is presently a Reader with the Department of Electronic and Electrical Engineering, Institute for Energy and Environment, University of Strathclyde. His research interests include power system protection; plant condition monitoring and intelligent asset management; applications of intelligent system techniques to power system monitoring, protection, and control; knowledge management; and decision support systems.